# Unified Push Recovery Fundamentals: Inspiration from Human Study

Christopher McGreavy, Kai Yuan, Daniel Gordon, Kang Tan, Wouter J Wolfslag, Sethu Vijayakumar, Zhibin Li

***Abstract*— Currently for balance recovery, humans outperform humanoid robots which use hand-designed controllers in terms of the diverse actions. This study aims to close this gap by finding core control principles that are shared across ankle, hip, toe and stepping strategies by formulating experiments to test human balance recoveries and define criteria to quantify the strategy in use. To reveal fundamental principles of balance strategies, our study shows that a minimum jerk controller can accurately replicate comparable human behaviour at the Centre of Mass level. Therefore, we formulate a general Model-Predictive Control (MPC) framework to produce recovery motions in any system, including legged machines, where the framework parameters are tuned for time-optimal performance in robotic systems.**

## I. Introduction

This paper investigates push recovery in humans and robots. Push recovery is segmented into a set of discrete strategies, each with a different method of control. In robotics, strategies are used in two ways: either as standalone push recovery controllers [1], [2], which useful against a small range of pushes, or combined into a single controller. Using a single controller which can combine all strategies is effective against a wider range of pushes [3], [4], but this often means there are sudden switches from one strategy to another [5]. Transferring between strategies, especially when each uses a different controller, can lead to failure cases. A second drawback is that users must select how much each action emerges during recovery [3]. Even with careful tuning, failures can occur when the tuned ratios do not match the needs of the recovery.

In contrast, humans combine strategies into continuous motions [6]. In humans, strategies are used in many combinations [7] and switches between them occur rapidly [8]. Thus it is unlikely that humans decide how strategies are used ahead of time or control each strategy differently, especially when sensory delays are considered.

Motivated by this human behaviour, we hypothesise that the discrete actions share fundamental principles which can be used as a unified controller across all strategies. For robotics this would mean tuning the emergence of each strategy is no longer required and reduces the need to use different controllers for each strategy.

### A. Related Work

The discrete push recovery actions are as follows:

This research is supported by the EPSRC CDT in Robotics and Autonomous Systems (EP/L016834/1).

The authors are with the Edinburgh Centre for Robotics and the School of Informatics, the University of Edinburgh, United Kingdom. Email: c.mcgreavy@ed.ac.uk

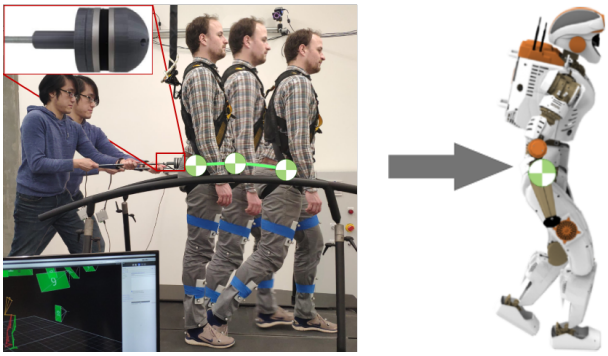

Fig. 1: Study of the common principles in human push recovery that lead to better robot control policies.

*Ankle Strategy* regulates ankle torque to modulate the Centre of Pressure (CoP) to affect CoM (Centre of Mass) motions for small pushes. Observed in humans [7] and used legged robots [1], this strategy is effectively modelled by the Linear Inverted Pendulum Model [9].

*Hip Strategy* applies torque at the hip joint to induce angular momentum around the CoM. This is observed in humans [10] and applied to robotics [1]. Though some work shows it has limited effect on recovery [11].

*Toe-Lift Strategy* generates upward CoM motions, and is prominent in humans [12]. The strategy has been applied in Robotics by controlling the under-actuated motion [13].

*Step Strategy* modulates the Support Polygon (SP) halting the CoM. Its effectiveness especially during large disturbances has been shown both in humans [6] and robots [2].

Discrete strategies can be combined using Model Predictive Control (MPC) [3] but parameter tuning dictates the desired emergence of strategies. Linear Quadratic Regulation [4] can effectively implement ankle and hip strategies by minimising joint deviations but does not include step strategy. Using a Proportional Integral Derivative as a CoM reference for Quadratic Programming (QP) whole-body control shows ankle and step strategies can emerge naturally [14]. Strategies can also emerge during learned locomotion [15].

As push recovery strategies appear simultaneously in humans [16], [8], we investigate this behaviour aiming to find shared principles of push recovery strategies. Applying this principle to robotics could reduce the number of parameters needed to tune recovery behaviour, since strategies would emerge naturally. To investigate these common principles, we first collect data of humans recovering from pushes. Data will be analysed to extract any common principles which may exist between the strategies. Lastly, we investigate how any principles might be adapted to use in robotics.

TABLE I: Threshold values for determining active strategies.

| Action | Criteria | Threshold | Human Max | Unit | Method |
|---|---|---|---|---|---|
| CoP | $p_{\text{heel,z}} \leq \delta_{\text{heel,z}}$ | $\delta_{\text{heel,z}} = 0.01$ | Variable | m | N/A |
| Angular Momentum | $L_t > \delta_t$ | $\delta_t = 0.1$ | 0.49 | s(Normalised) | Torso sway with feet fixed to ground |
| CoM Height | $\dot{z} > \delta_{\dot{z}}$ | $\delta_{\dot{z}} = 0.02$ | 0.1269 | m/s | Stand on toes as quickly as possible |
| Support Polygon | $p_{\text{toe,z}} > \delta_{\text{s},v_{\text{L,R}}} > \delta_{\text{s}}$ | $\delta_{\text{s}} = 0$ | N/A | N/A | N/A |

Notation: $p_{\text{heel,z}}$ Heel height, $L_t$ Hip Angular Momentum, $\dot{z}$ CoM Velocity (Z Axis), $p_{\text{toe},z}$ Toe Height, $v_{\text{L,R}}$ Foot Velocity (X Axis) $\delta_{\text{heel,z}}$ Heel Height Threshold, $\delta_t$ Hip Angular Mom. Threshold, $\delta_{\dot{z}}$ CoM Height Threshold, $\delta_s$ Step Threshold

### B. Contributions

This work presents the following contributions:

1) Experimental design extracting useful physical quantities to identify recovery strategies in humans
2) Classification criteria of human push recovery strategies
3) Evidence of minimum jerk regularisation as core strategy during push recovery.
4) Control design of a minimum jerk controller that resembles human CoM behaviour
5) Application of extracted core principles to robotics controller with better performance.

In this paper, we describe our experimental method (Sec II), define criteria for identifying recovery strategies (Section III). Using this data, Section IV presents common principles across strategies, followed by results (Section V) and validation of the principle and our conclusions (Section VI).

## II. Experimental Setup and Data Collection of Human Experiments

Following, the experimental setup to understand human push recovery, identify control parameters, and obtain a baseline controller performance will be presented.

### A. Subjects

We collected 60 trials from 4 participants recruited from the University of Edinburgh. Ethics approval was gained. Each subject gave written informed consent before testing.

### B. Equipment

A mounted force/torque sensor (Figure 1 inset) was used to push subjects and measure the applied force. VICON motion tracking recorded the movement of optical markers. A template of human body mass distribution was scaled to each participant in OpenSim [17]. This was used to calculate CoM position, joint angles, positions and body dimensions used to calculate angular momentum [18].

### C. Experimental Design

Each participant underwent 15 push trials. Instructions were to try to return to the initial position after the push. If a step was required, they were told to come to a stop and not attempt to return to the initial position. Illustrated in Figure 1, participants were pushed at the coccyx using the force/torque device. Pushes, with magnitude and timing unknown to the subjects, were applied after 2-3s of quiet standing followed by a recovery action of the subject. To ensure purely reactionary responses without sensory cues, pushes were applied by experimenters. Impulses were varied and ranged from $12.1\,\text{N}\,\text{s}$ to $55.5\,\text{N}\,\text{s}$, with a mean and standard deviation of $35.9\,\text{N}\,\text{s}$ and $10.3\,\text{N}\,\text{s}$.

### D. Data Considerations and Post Processing

Recovery begins after the push force is removed and ends when stability is regained. Motion capture data is trimmed to remove movement when force sensor readings are below 2N and after recovery has ended. Only sagittal movement is considered as all pushes were performed in the sagittal plane. Velocity, acceleration, and jerk were obtained through differentiation of marker positions from motion capture. CoM states are normalised by leg length and unitless. Low-pass filtering was applied to denoise all data (4th order Butterworth, cut-off frequency at 6Hz).

## III. Strategy Identification Criteria

We define *Control Actions* as the active component for recovery, e.g., CoP modulation, and use the term *Strategies* as label for an entire recovery trial. *Strategy* labels denote the highest *Control Action* that was used during a trial. To identify Strategies in the data, we determine the Control Actions from a set of criteria and thresholds (Table I).

Since multiple recovery strategies simultaneously, we use the nomenclature of *Control Actions* and recovery *Strategies* to distinguish between discrete methods of recovery and a label for an entire recovery trial respectively. The discrete push recovery actions discussed in Section I-A are all based on a single active component. For example, the active component of the ankle strategy is manipulating the CoP. The criteria in Table I can then be used to identify which control actions are active at each timestep of a recovery trial. *Strategy* labels denote the highest *Control Action* that was used during a trial. Control Actions are ranked by the maximum normalised impulse rejected during each trial (Table II). By making this distinction, we can qualitatively investigate how humans perform push recovery. This will add to the evidence that humans are unlikely to pre-select discrete recovery motions or use different policies to control them. The mean CoM trajectories for each Strategy are plotted in Figure 5.

TABLE II: Max normalised impulse observed in each action.

| Rank | Action | Impulse [ms] |
|---|---|---|
| 1 | CoP Modulation | 52 |
| 2 | Angular Momentum Modulation | 59 |
| 3 | CoM Height Modulation | 72 |
| 4 | SP Modulation | 77 |

### A. Relationship Between Control Actions and Strategies

The dependence of control actions on the push magnitude are shown in Figure 2. Since subjects cannot predict the push force in advance, they gradually employ increasingly more effective techniques: lower ranked actions are used

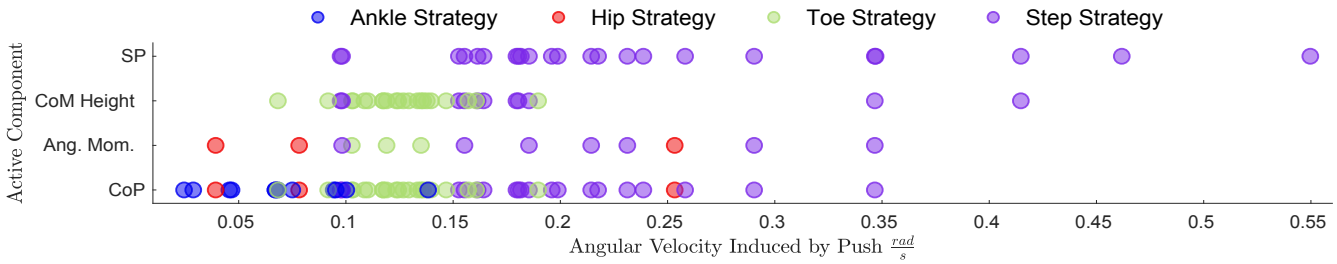


Fig. 2: Active components of strategies (y axis, circles) appear at different frequencies depending on the angular velocity (CoM w.r.t the ankle) caused by a push. Each colour shows which main strategy is used in that trial. Vertically aligned circles also represent a single trial, though connecting lines were removed for visibility. Push magnitude is represented by the caused angular momentum around subjects' ankles.

for smaller pushes and more actions are incorporated as the magnitude increases. For large pushes, weaker actions are skipped completely, and subjects immediately use higher ranked actions. The further the CoM diverge from the equilibrium (*i.e.* quiet standing), the stronger the Control Actions (blue boxes) become (Figure 3).

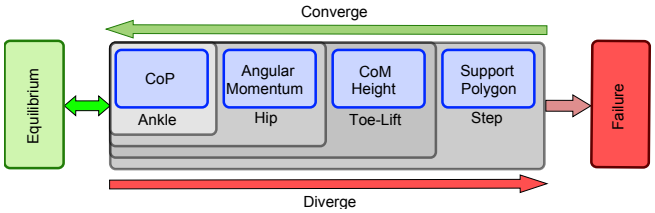


Fig. 3: Relationship between control actions and strategies. As a system diverges from the equilibrium, a sequence of control actions (blue) will be activated. A strategy is defined by the highest active/dominant control action (grey gradient).

### B. Stability regions

Through calculating a set of stability regions, which represent which actions can affect the CoM in a given state, we can identify their effectiveness and when they are used. We calculate these regions for humans and for an example robot with robot values using the specifications of the Valkyrie robot and human values obtained experimentally (Table III).

By adding physical constraints to a subject, we sequentially isolate the effect of each action. CoP Modulation parameters are obtained from the mean foot length among participants. The Angular Momentum Modulation constraints $\tau_{\max}$ are determined by fixing the subject's heels to the ground enabling only hip recovery behaviour and increasing push forces until recovery using the hip was no longer possible. CoM Height Modulation parameters were obtained as in Section III. For identifying the constraints during Support Polygon Modulation increasing pushes were applied until a flight phase was needed to recover. Stability regions are defined at the CoM initial state $\boldsymbol{x}_0 = [x_0, \dot{x}_0]$ and are calculated for each action. An action can stabilise the system if $\boldsymbol{x}_0$ is in its stability region (Fig. 4).

*1) CoP Modulation:* To remain stable whilst balancing, the CP must lie within the Support Polygon:

$$p_{\min} \leq x + \dot{x}\omega \leq p_{\max}, \tag{1}$$

where $\omega = \sqrt{g/z_c}$, and foot dimension (support polygon bounds) $p_{\min}, p_{\max}$. This bound is more practical than the ZMP criterion [19], as the CoM must be within the SP at the end of the recovery (at $t \to \infty$). The CP can then be controlled by modulating the CoP within the SP using the dynamics of the LIP model [9].

*2) Angular Momentum Modulation:* This action allows additional control via torque around the CoM, thus expanding the Capturability Region [2]:

$$p_{\min} - \alpha \leq x + \omega\dot{x} \leq p_{\max} + \alpha, \tag{2}$$

with $\alpha = \frac{\tau_{\max}}{\beta^2 mg}(\beta - 1)^2$, $\beta = e^{\omega T_{\max}}$, mass $m$, gravity constant $g$, maximal torso actuator torque $\tau_{\max}$, $\omega = \sqrt{g/z_c}$, maximum time $T_{\max} = \sqrt{4I/\tau_{\max}(\theta_{\max}) - \theta_0)}$, inertia $I$, maximal torso angle $\theta_{\max}$ and starting angle $\theta_0$.

*3) CoM Height Modulation:* This control action increases virtual leg length, e.g., through toe-tilting, and provides a force $f$ perpendicular to the COM velocity that reduces the horizontal velocity $\dot{x}$. To find the Stability Region for toe-tilting, we need to analyse whether horizontal CoM velocity can be reduced to zero at the edge of the foot.

The horizontal velocity $\dot{x}_0$ is induced by external pushes, while the vertical velocity $\dot{z}(x_0, \dot{x}_0)$ can be added through CoM Height Modulation. We assume that COM motion will follow a straight line from initial condition $[-x_0, z_c]$ to endpoint $[0, z_c + \Delta z_{\max}]$. This over-approximates the Stability Region by assuming that the required force $f$ can be generated at all times. For a more conservative estimation, a stability margin for the endpoint can be set instead of letting it be at the edge of the foot.

To achieve a straight line, a vertical velocity $\dot{z}$ needs to be set:

$$\dot{z}(x_0, \dot{x}_0) = \sqrt{\frac{\Delta z_{\max}^2 \dot{x}_0}{(x^2 + \Delta z_{\max}^2)(1 - \frac{\Delta z_{\max}^2}{x_0^2 + \Delta z_{\max}^2})}}, \tag{3}$$

while not exceeding the physical capabilities of the robot:

$$\dot{z}(x_0, \dot{x}_0) \leq \dot{z}_{\max}. \tag{4}$$

Due to $f$ being perpendicular to the COM velocity, we can energy balance to compute velocity at the foot edge. At this point $E_{\text{kinetic}} \leq \Delta E_{\text{potential}}$ must hold with $E_{\text{kinetic}} = \frac{1}{2}m(\dot{x} + \dot{z}(x_0, \dot{x}_0))^2$, and $\Delta E_{\text{potential}} = mg\Delta z_{\max}$. If this constraint is not met, the robot will pivot around the toe and fall.

TABLE III: Physical properties required for calculating balance limits and their associated boundaries.

| | COP Modulation | | Angular Momentum Modulation | | COM height Modulation | | Support Polygon Modulation | | |
|---|---|---|---|---|---|---|---|---|---|
| | $p_{\min}$ [m] | $p_{\max}$ [m] | $\theta_{\max}$ [rad] | $\tau_{\max}$ [Nm] | $v_{z,\max}$ $[\frac{\text{m}}{\text{s}}]$ | $z_{\max}$ [m] | Step Length [m] | $v_{\min}$ $[\frac{\text{m}}{\text{s}}]$ | $v_{\max}$ $[\frac{\text{m}}{\text{s}}]$ |
| Human | 0.10 | 0.17 | 0.27 | 3.01 | 0.13 | 0.13 | 0.5 | 0.1 | 3.95 |
| Robot | 0.12 | 0.19 | 0.66 | 150 | 0.10 | 0.07 | 0.25 | 0.1 | 3.00 |

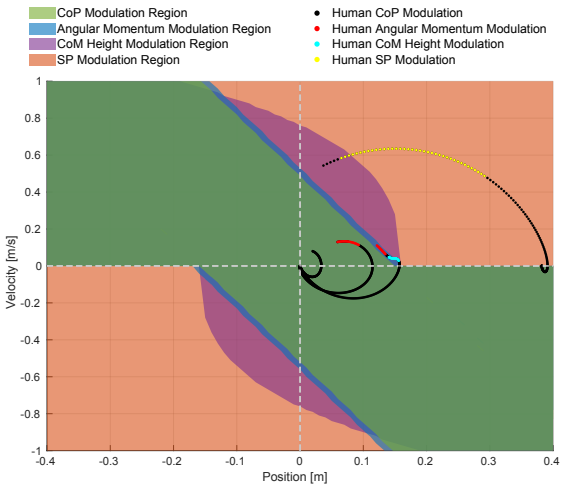


Fig. 4: Stability regions for each action with coloured curves indicating human CoM motion during recovery trials.

*4) Support Polygon Modulation:* The stability region is gained using the controller proposed in Section IV-B.1 with a given initial CoM state. If for the given initial condition, the robot can halt using the given constraints, then the initial condition is in the stability region.

Figure 4 shows these stability regions in relation to human CoM trajectories and Control Actions. The approximate stability regions are a close match to the Actions (coloured dots) shown in human movement. In the non-stepping cases, the CoM remains in the original support polygon, whereas in the stepping case, the CoM diverges to a new SP.

## IV. CoM Behaviour During Recovery Strategies

Following, we present a single control principle matching trajectories across push recovery actions and strategies without a switching mechanism between Control Actions.

### A. CoM Modelling

From our human motion analysis, a dominating effects of the CoM dynamics was observed. Hence, we use a point mass model which is in agreement with past study [20] to analyse human CoM data, and to find the fundamental principles between the strategies:

$$\frac{\mathrm{d}^3}{\mathrm{d}t^3}x = u, \tag{5}$$

where $x$ is CoM position and the controlled variable $u$ is CoM jerk $\dddot{x}$. The model assumes the required control input $u$ can be produced by the Ground Reaction Forces (GRF). This assumption will be ensured by constraining the input in the MPC. An independent integrator model is used for each axis, horizontal and vertical.

### B. Minimum Jerk Model Predictive Control (MJMPC)

Our aim is to find a single control principle which accurately matches measured human trajectories in all strategies.

*1) Model-Predictive Control Formulation:* A minimum jerk principle is used as the single principle control principle to investigate fit across strategies. The strong resemblance between the human data and minimum jerk trajectories often used to explain human motions [21] motivates this decision. A minimum jerk MPC controller is designed, which minimises the objective function:

$$C(u(t)) = \frac{1}{2}\int_0^{t_f}\left(\frac{\mathrm{d}^3x(t)}{\mathrm{d}t^3}\right)^2 dt = \frac{1}{2}\int_0^{t_f} u(t)^2\mathrm{d}t. \tag{6}$$

Jerk $\frac{\mathrm{d}^3x}{\mathrm{d}t^3}$ is used as control effort $u$ with final time $t_f$. The MPC solves the following constrained optimisation problem:

$$\begin{aligned}
&\min_{u(t)} && C(u(t)) \\
&\text{subject to} && \text{Eq. 5} \\
& && [x(0), \dot{x}(0), \ddot{x}(0)] = [x_0, \dot{x}_0, \ddot{x}_0] && (7)\\
& && [x(t_f), \dot{x}(t_f), \ddot{x}(t_f)] = [x_f, \dot{x}_f, \ddot{x}_f] && (8)\\
& && [x_{\min}, \dot{x}_{\min}, \ddot{x}_{\min}] \leq [x, \dot{x}, \ddot{x}] \leq [x_{\max}, \dot{x}_{\max}, \ddot{x}_{\max}], && (9)
\end{aligned}$$

with initial condition $[x_0, \dot{x}_0, \ddot{x}_0]$, terminal condition $[x_f, \dot{x}_f, \ddot{x}_f]$, and eq. 9 for physical feasibility.

In the MJMPC scheme (Algorithm 1), first, the desired CoM states $X_{\text{des}}$, $Z_{\text{des}}$ are set as terminal conditions in the constrained optimisation problem. While the desired CoM height stays constant, the desired horizontal CoM $x_d$ is computed by the step optimiser (Section IV-C.2) if the CP exceeds the SP. Using the current state as the initial condition $X_0, Z_0$ and the final time $t_f$ (Section IV-C.3), the control effort $u_{x,1:t_f}, u_{z,1:t_f}$ is calculated over prediction horizon $t_f$ by solving the constrained optimisation (7). Lastly, a whole-body QP controller calculates feasible joint torques $\tau$ by executing the first CoM reference position gained by minimising CoM jerk value $X_{\text{ref}} \leftarrow X_{\text{ref},1:t_f}(1)$ from the whole control input trajectory $u_{i,1:t_f}$ in an MPC fashion.

Although Angular Momentum Modulation was present in the human data, we found that by using two linear point models, we were able to recreate CoM motion during hip strategy needing to control Angular Momentum.

### C. Optimising Parameters to Fit Human Data

Three components are required before these controllers can be fitted to human trajectories: initial condition $\boldsymbol{x}_0$, terminal condition $\boldsymbol{x}_f$ and hyperparameters of each controller.

*1) Initial Conditions:* The parameters will be fit across all human trials using the CoM state at the moment the push is removed as the initial condition $\boldsymbol{x}_0$ for each trial.

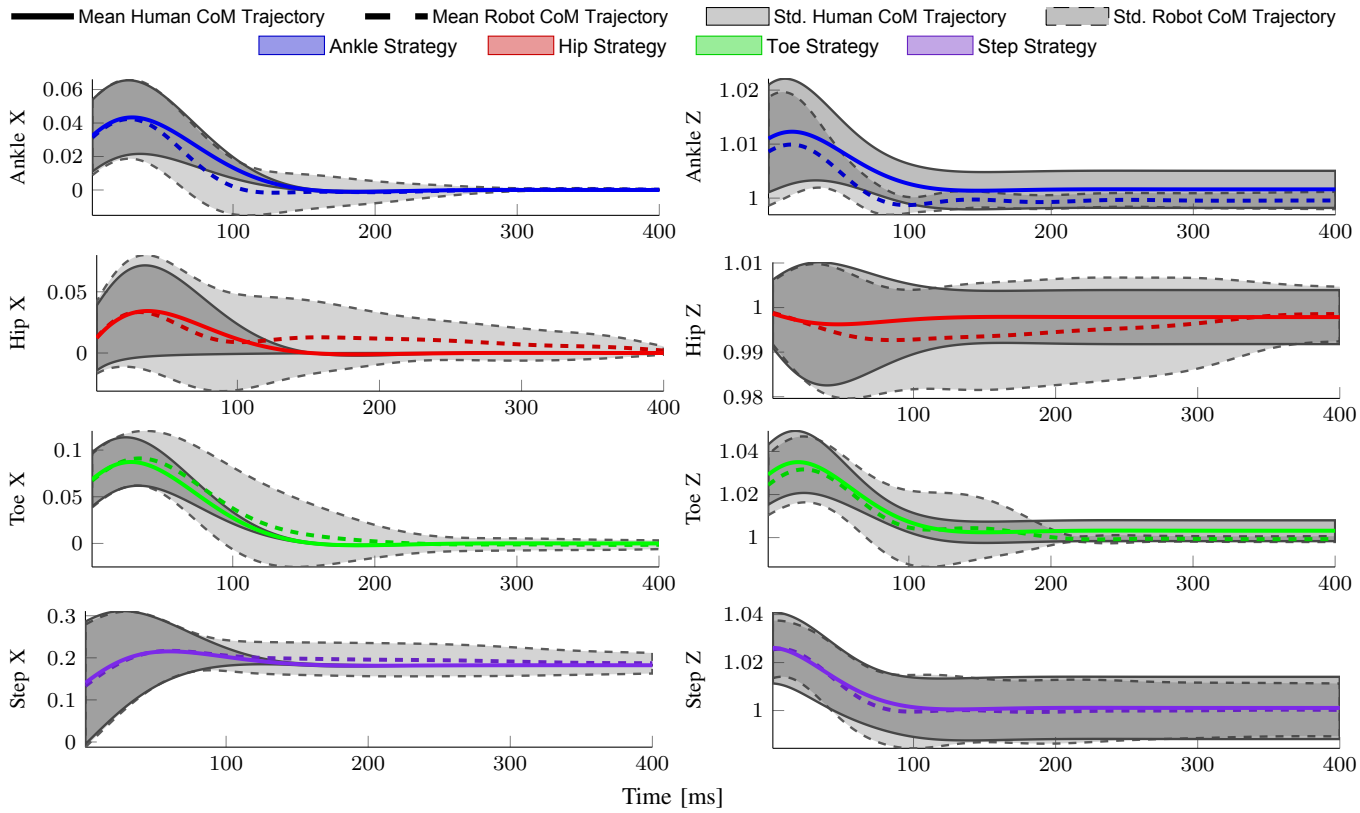


Fig. 5: Comparison of human (solid line) and robot (dashed line) performance. Rows: ankle, hip, toe, step strategies in X and Z axes (columns). Units: leg length $l$.

**Algorithm 1** Algorithm for MJMPC

$X_{\text{des}} \leftarrow [0,0,0]^T$, $Z_{\text{des}} \leftarrow [z_c,0,0]^T$
**while** $X \neq X_{\text{des}}$ **do**
  **if** $CP > SP$ **then**
    $X_{\text{des}} \leftarrow step\_optimiser(X)$
  **end if**
  $X_0 \leftarrow X$, $Z_0 \leftarrow Z$
  $X_{\text{ref}} \leftarrow \min_{u(t)} f(u(t))$
  $X_{\text{ref}} \leftarrow X_{ref,1:t_f}(1)$
  $Z_{\text{ref}} \leftarrow \min_{u(t)} f(u(t))$
  $Z_{\text{ref}} \leftarrow Z_{ref,1:t_f}(1)$
  $\tau \leftarrow$ Whole Body Control($X_{\text{ref}}, Z_{\text{ref}}$)
  $X, Z \leftarrow$ Robot($\tau$)
**end while**

*2) Terminal Conditions:* The reference state $\boldsymbol{x}_f = [0,0,0]^T$ as the terminal condition is applied to all non-stepping actions. For stepping actions, a new CoM reference is required, which is provided by the optimisation method for foot placement presented in [22]. This step optimisation considers kinematic and dynamic limits of the physical system as inequality constraints and outputs a new step location which is the final CoM position $x_d$, yielding the terminal constraint as $\boldsymbol{x}_f = [x_d,0,0]$. Step are only taken when the CP is beyond the SP. Our collected human data only involve a single step, but this can be extended to multiple steps for large pushes.

TABLE IV: Comparing controller & human trajectories.

| Axis | Mean MSE [mm$^2$] | | | | |
|---|---|---|---|---|---|
| | Ankle | Hip | Toe | Step | Total |
| X | 0.022 | 0.075 | 0.623 | 0.560 | 0.366 |
| Z | 0.003 | 0.005 | 0.07 | 0.01 | 0.0257 |

*3) Final Time:* The hyperparameters for each controller are determined via the least square fitting. The fitting minimises the least square error between the CoM trajectory generated by humans $Y$ and controller $Y^*$, given the controller-specific parameters $P$ at each time step $t$:

$$\sum_{i=1}^{N}\sum_{t=1}^{T}(Y^*_{t,i}(P) - Y_{t,i})^2. \tag{10}$$

Optimisation was performed using the MATLAB `fmincon`, and $t_f$ was fit to both the X and Z axes for all trials.

## V. Results

We present fitting results to the human data, and analyse the stability regions of the generated motions.

### A. Characterising Human Data

Applying MJMPC with a fitted prediction horizon of 123 ms and 101 ms for the X and Z axis respectively, a close fit between human data and controller was achieved (Table IV). The controller has a total Mean Square Error over all trials of 0.366mm$^2$ and 0.0257mm$^2$ for X and Z axis respectively. The MJMPC scheme's ability to closely characterise the

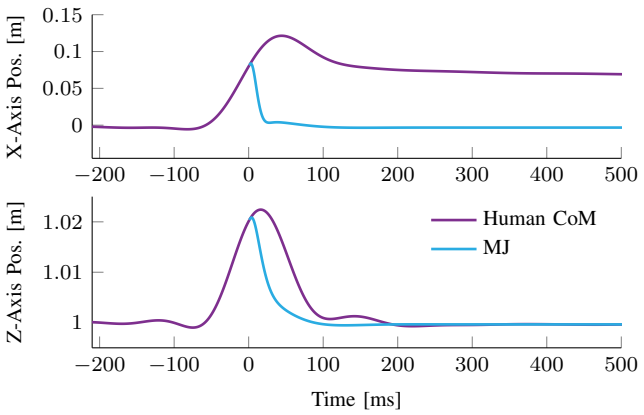


Fig. 6: CoM trajectories tuned for time optimal performance. Compared to humans MJMPC converges faster and does not step to recover from the push.

human policy can be seen by the close resemblance between human and robot trajectories (Figure 5).

### B. Applying Push Recovery Principles to Robotics

Having shown a single control principle can be used to explain human CoM motion across the main push recovery strategies, we show this can be used for robotics. In the earlier section, we used the MJMPC controller to match human performance. Our goal, however, is not to blindly imitate human behaviour, but to extract useful principles from humans such that they can be used in robotics. By tuning the time parameter of the MJMPC such that the CoM reaches the desired state as quickly as possible, we may see better performance while being able to exhibit each of the strategies. The reformulated control objective uses a time-optimal-like control cost, subject to force and torque limits of our example robot in Table III:

$$\min_{x(t),z(t)} \quad \frac{1}{2}\int_0^{t_f} ((x_d(t)-x(t))+(z_d(t)-z(t)))^2 \mathrm{d}t \quad (11)$$

$$\text{subject to:} \quad \tau \leq \tau_{\max}, \quad F \leq F_{\max} \quad (12)$$

where $x(d), z(d)$ are the desired positions for the controller, set to the initial position of the human CoM during quiet standing before the push starts. This output is constrained to ensure the torque $\tau$ and force $F$ produced are within the robot's limits $\tau_{max}, F_{max}$ If the CP moves out of the SP, the same step selection criteria as in IV-C were used.

Figure 6 shows the performance of the MJMPC using the new parameters with mean human CoM behaviour for comparison. We see, that the mean human trajectory after being pushed diverges significantly from the initial position, caused by human subjects taking a step. In contrast, MJMPC can return to the initial position without stepping, since the calculated CP does not move outside the SP (Alg:1, Ln:3).

When we were fitting the controllers to the human CoM trajectories in the previous section, the controllers were implicitly accounting for sensing and muscle actuation delays in humans. Since these delays are trivial in robotics, using this time optimal approach, we can achieve higher performance than in the human data.

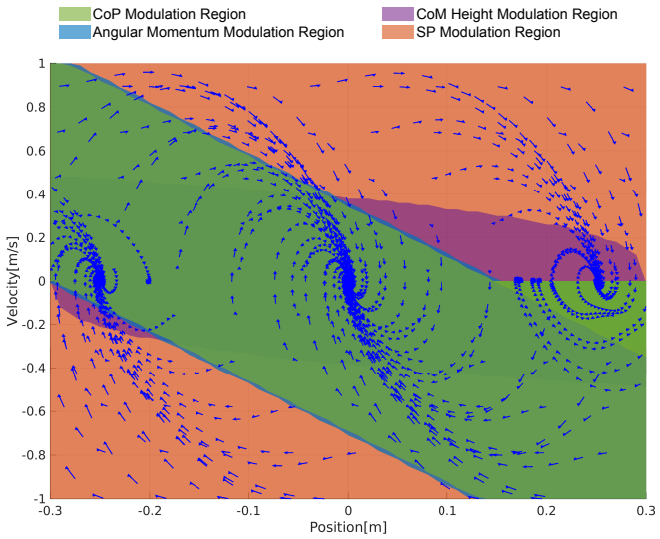


Fig. 7: MJMPC regions of attraction. Arrows show the trajectories from a grid of initial conditions. When in stepping regions they converge at step locations from Section IV-C.

### C. Comparing Stability Region between Human and Robots

The boundaries defined in Section III-B are used to generate stability regions for robots (Fig. 7) using the values in Table III. The robot stability regions are qualitatively similar to human regions in 4. Furthermore, the low effectiveness of Angular Momentum Modulation can be seen through its stability region in both human and robot plots. It largely overlaps with the CoP Modulation, and in most cases is within the CoM height modulation stability region. This indicates that the Angular Momentum Modulation is, in fact, replaceable by a combination of CoP and CoM Height modulations, and human data was indeed well reconstructed using this approach as shown in Section V-A.

## VI. Conclusion

This paper first investigated human push recovery motions. We quantified a set of criteria which can identify when Control Actions are being used. Once these were identified, we were able to find a common minimum jerk control principle which could accurately match each of these Control Actions. Taking this control principle, we were then able to increase performance by tuning its parameters to perform optimally rather than to fit human data.

From this, we conclude that despite the apparent complexity of human recovery behaviour, by focusing on the CoM, a simple core rule can account for the wide variety of motion. In studying human push recovery, we obtain a warm-start to show effective ways of exploring complex movement problems in robotics. Adapting these principles also has value in robotics. As a next step, we will validate feasible recovery motions on a real system performed by the controller while undergoing a series of pushes. Furthermore, future work will study more complex motor skills from humans, such as fall recovery and climbing, and investigate new framework and approaches to transfer more human-level skills to robots.

## REFERENCES


[1] B. Stephens, "Humanoid push recovery," in *IEEE-RAS Int. Conf. on Humanoid Robots*, 2007.

[2] J. Pratt, *et al.*, "Capture point: A step toward humanoid push recovery," in *IEEE Int. Conf. on Humanoid Robots*, 2006.

[3] Z. Aftab, *et al.*, "Ankle, hip and stepping strategies for humanoid balance recovery with a single model predictive control scheme," in *IEE Int. Conf. on Humanoid Robots 2012*.

[4] C. G. Atkeson and B. Stephens, "Multiple balance strategies from one optimization criterion," in *IEEE Int. Conf. on Humanoid Robots 2007*.

[5] L. Kaul and T. Asfour, "Human Push-Recovery:Strategy Selection Based on Push Intensity Estimation," *Int. Symp. on Robotics*, 2016.

[6] H. Hoffmann, *et al.*, "Biologically-inspired dynamical systems for movement generation: Automatic real-time goal adaptation and obstacle avoidance," *IEEE Int. Conf. on Robotics and Automation 2009*.

[7] L. M. Nashner and G. McCollum, "The organization of human postural movements: a formal basis and experimental synthesis," *Behavioral and brain sciences*, 1985.

[8] Y.-C. Pai and J. Patton, "Center of mass velocity-position predictions for balance control," *Journal of biomechanics*, 1997.

[9] S. Kajita and K. Tani, "Study of dynamic biped locomotion on rugged terrain-derivation and application of the linear inverted pendulum model," *IEEE Int. Conf. on Robotics and Automation*, 1991.

[10] J. Allum and F. Honegger, "Interactions between vestibular and proprioceptive inputs triggering and modulating human balance-correcting responses differ across muscles," *Experimental brain research*, 1998.

[11] P. Zaytsev, *et al.*, "The boundaries of walking stability: viability and controllability of simple models," *IEEE Trans. on Robotics*, 2018.

[12] K. B. Cheng, *et al.*, "Role of heel lifting in standing balance recovery: A simulation study," *Journal of Biomechanics*, 2018.

[13] Z. Li, *et al.*, "Humanoid balancing behavior featured by underactuated foot motion," *IEEE Transactions on Robotics*, 2017.

[14] K. Seo, *et al.*, "Towards natural bipedal walking: Virtual gravity compensation and capture point control," in *IEEE Int. Conf. on Intelligent Robots and Systems*, 2012.

[15] C. Yang, *et al.*, "Learning whole-body motor skills for humanoids," in *IEEE-RAS Int. Conf. on Humanoid Robots 2018*.

[16] A. Hofmann, "Computer Science and Artificial Intelligence Laboratory Technical Report Robust Execution of Bipedal Walking Tasks From Biomechanical Principles," 2006.

[17] S. L. Delp, *et al.*, "Opensim: open-source software to create and analyze dynamic simulations of movement," *IEEE transactions on biomedical engineering*, 2007.

[18] D. Gordon, *et al.*, "Effectively quantifying the performance of lower-limb exoskeletons over a range of walking conditions," *Frontiers in Robotics and AI*, 2018.

[19] S. Kajita, *et al.*, "Biped walking pattern generation by using preview control of zero-moment point," *IEEE Int. Conf. on Robotics and Automation*, 2003.

[20] Z. Li, *et al.*, "Comparison study of two inverted pendulum models for balance recovery," in *2014 IEEE-RAS International Conference on Humanoid Robots*, 2014, pp. 67–72.

[21] T. Flash and N. Hogan, "The coordination of arm movements: an experimentally confirmed mathematical model," *Jrnl of neuroscience*, 1985.

[22] W. Hu, *et al.*, "Comparison study of nonlinear optimization of step durations and foot placement for dynamic walking," *IEEE Int. Conf. on Robotics and Automation*, 2018.